Al-Nahrain Journal of Science
ANJS, Vol.28 (4), December, 2025, pp. 173-187

Photo-Thermal Conversion of Selective Coatings with Iron and Chromium Powder Additives

Mohammed Al-Ameen Amer, Ahmed A. Al-Tabbakh*

Department of Physics, College of Science, Al-Nahrain University, Jadiriya, Baghdad, Iraq

Article's Information

Received: 12.07.2025
Accepted: 23.09.2025
Published: 15.12.2025

Keywords:
Solar collectors,
Coating,
Photo-thermal effect,
Optical absorption,
Nanopowders.

Abstract

In the present work improvement of the solar-to-thermal conversion in aluminum substrates coated with heat-resistant black paint and enhanced by iron (Fe) and chromium (Cr) powders was attempted. Aluminum sheets were cleaned and coated with a commercial black paint. On the top of the primary paint Fe and Cr powders (both individually and combined) were applied using an air-spraying method. The morphology and uniformity of coatings were examined using optical and scanning electron microscopes. The coating elemental makeup was investigated using energy-dispersive X-ray spectrometer (EDS). The capability of the photo-thermal conversion was tested by exposing the coated substrates to solar radiation in collector setup. The substrate temperature was monitored over time. The reflectance measurements were conducted using a pyrheliometer-like device. The spectral absorptance was determined and analyzed via UV-Vis spectroscopy measurements. The elemental analysis confirmed the effective and homogeneous incorporation of the iron and chromium powders into the coatings. A minor cross-contamination was attributed to the processing of the coatings. Results show that by adding Fe and Cr powders a notable change in the surface morphology was observed. This has led to increase in the roughness and complexity of the coating surface. This roughness was a key parameter for light trapping and absorption. Among the coatings investigated, the Fe-modified sample showed the highest solar absorptance (96.23%) and greatest temperature increase under irradiation, surpassing both the Cr-modified and combined Fe+Cr coatings. The UV-Vis analysis revealed that Fe-containing coatings possessed the greatest integrated absorbance, especially within the visible spectrum (500–800 nm), aligning with their superior photo-thermal performance. These results highlight that integrating Fe powder into heat-resistant paint can be an effective and practical approach to optimize the solar-to-thermal energy conversion. Such approach offers promising application in solar thermal collectors.

http://doi.org/10.22401/ANJS.28.4.14
*Corresponding author: tabbakh2013@gmail.com

1. Introduction

Solar-thermal collectors are devices designed to harness solar radiation and transform it into heat energy. They have variety of designs and configurations and serve numerous applications in industrial and residential settings. Common uses of solar collectors include heating of spaces, swimming pools and domestic water. In addition, collectors may be used for generation of steam and for water desalination [1-8]. Beyond these applications, solar-thermal technology is also applied in more specific fields such as bacterial sterilization, catalysis, and sensing [9, 10]. The performance of concentrated and non-concentrated solar collectors, whether for home or industrial use, largely depends on the selective coatings applied to their surfaces. These coatings are the key element in converting the incoming solar radiation into thermal energy. The efficiency of this conversion is influenced by the coatings' structural, elemental, geometric, and physical properties [11, 12]. Modern selective coatings may incorporate nanomaterials and nanostructures to enhance their

absorption capabilities. Such designs aim to maximize the absorption of solar radiation while minimizing reflectance. This is accomplished by promoting mechanisms like radiation trapping. Effective coatings must exhibit low thermal emissivity to reduce energy loss at moderate to high operating temperatures. Such coatings may consist of single or multiple layers, which can be either thin or thick films. A wide range of materials is used in these coatings for direct solar energy conversion, including innovative substances like multiwall carbon nanotubes, which contribute to improved overall performance [13-15]. Currently, our research focuses on exploring alternative materials to enhance the photo-thermal conversion efficiency of commercially available coatings. Specifically, we aim to improve solar-to-thermal energy conversion by incorporating micro- and sub-micro particles into black paint formulations. The main goal is engineering surface morphologies that increase radiation trapping. Earlier studies concentrated on particles such as carbon powder and lithium metal oxide [16, 17]. Two metals have been chosen for this application: iron and chromium. Fernandez et al. conducted a systematic study on the photo-thermal properties of iron nanoparticles with a range of sizes, shapes and surface coatings [18]. These nanoparticles were synthesized via various chemical methods and characterized for their morphology, size, and optical behavior. They found that particle size, shape, and surface coating play a significant role in determining photo-thermal heating efficiency. They noted that octahedral particles of approximately 32 nm in size with dextran coating exhibit pronounced photo-thermal effects. This work offers a comprehensive and methodical assessment of how the characteristics of Fe-based nanoparticles influence photo-thermal conversion, providing valuable insights for optimizing Fe-containing coatings. However, the results may have limited applicability to large-area coatings or non-biological settings, which is the focus of the present study. Chromium and its oxides have been identified as key materials in the advancement of high-performance solar thermal collectors, particularly for use in concentrated solar power systems [11]. These materials are distinguished by their exceptional thermal and chemical stability at elevated temperatures, as well as their outstanding corrosion resistance. Additionally, chromium-based coatings possess favorable optical characteristics, such as high solar absorptance and low thermal emittance, both of which are essential for efficient photo-thermal conversion. Cermet coatings containing chromium are frequently recommended for parabolic trough collectors and other types of concentrated solar collectors. Furthermore, multilayer and composite structures based on chromium—such as Cr/Cr_2O_3 and CrN/Cr_2O_3—are specifically engineered to optimize solar absorptance while minimizing thermal emittance. This enhances the overall efficiency of the solar selective coatings. It is worth mentioning that both metals are abundant and cost-effective compared to noble metals. They are considered ideal candidates for scalable and sustainable photo-thermal coatings. The presence of iron and its oxide phases enhances solar absorptivity and thermal stability significantly facilitating efficient conversion of solar radiation into heat. Conversely, owing to the formation of a protective oxide layer on its surface, chromium offers superior corrosion resistance compared to iron which forms more porous oxide layer. Chromium exhibits better mechanical properties than iron despite its slightly lower density. The purpose of combining chromium (Cr) and iron (Fe) powders with commercial black paint is to enhance the paint's optical and photo-thermal properties. Cr and Fe powders do not react spontaneously under normal conditions, as both form protective oxide layers that prevent interaction. This study explores an easy approach to preparing coatings with reduced processing steps and heat treatment. The novelty of this work lies in the enhanced absorptance achieved by incorporating Fe powder into the heat-resistant paint, combined with the ease of applying the coating regardless of the substrate's area or geometry.

2. Materials and Methods

In this work, the substrates were prepared from aluminum sheets with a thickness of 1 mm and moderate purity of ~95%. The substrate had dimensions of 4.5 cm by 4.5 cm. Each substrate underwent a series of cleaning steps, starting with mechanical abrasion, brushing, and degreasing, to eliminate surface contaminants. The cleaning process involved washing the substrates with detergent. After that, each substrate was thoroughly rinsed with deionized water. Then they were soaked in acetone to remove any residual grease or impurities. After these treatments, the substrates were air dried. While the impact of surface cleanliness on factors like paint adhesion and other functional properties is not addressed in this work, the adopted cleaning protocol is considered sufficient for the intended experiments and measurements. This method is both practical and economical for treating larger surfaces. Prior to applying the

coatings, the substrates were dried by placing them in a furnace. The primary coating consisted of a heat-resistant black paint manufactured by Rust-Oleum Corporation, USA. This particular paint has been employed in previous studies and demonstrated compatibility with a variety of additives, facilitating their even dispersion. Additionally, it performs well under low to moderate temperature conditions and possesses anti-cracking properties. This will be discussed in this presentation. Key specifications of the paint are summarized in Table 1. Photographs of the substrates, taken with a standard camera before and after coating, are presented in Figure 1 (a–d). Two powders, iron and chromium, were separately and collectively incorporated into the high-resistance paint. The powders were added on top of the coating surface using an air-spraying technique. Initially, the powders were loaded into the spraying apparatus. Following the application of the high-resistance paint, the powders were sprayed from a distance of at least 30 cm while the substrate was gradually rotated. This rotation helped preventing the particles from settling in one direction and ensured a more uniform distribution of the powder across the substrate surface.

Table 1: Specifications of the primary coating.

Property	Black coating
Resin type	V2178838 ROHPER +LSPR 6PK FLAT BLACK
Pigment type	ROHPER +LSPR 6PK FLAT BLACK
Solvent	Acetone, Xylene, Toluene and liquid petroleum gas propellant
Dry time at 10-32 °C and 65% relative humidity	1-2 hours
Relative density with respect to water	0.821
Dry heat resistance	538 °C
Storage	49 C°
Specific Gravity	0.824

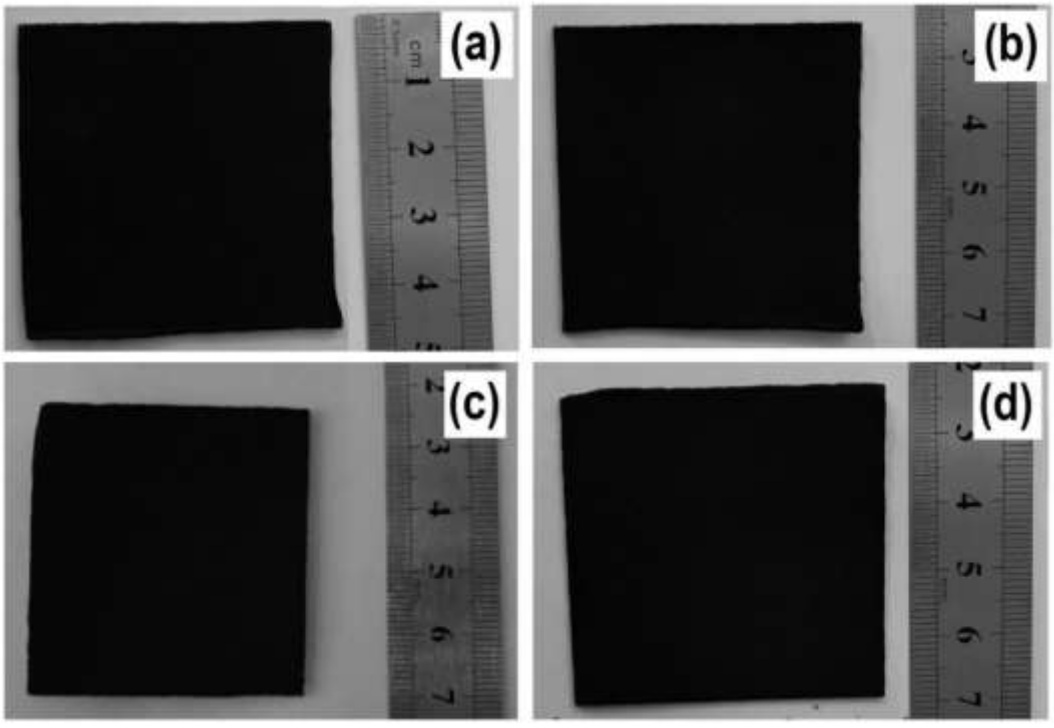

Figure 1: The Al substrates after being coated with (a) heat-resistant black paint (HRBP) (b) Fe/HRBP (c) Cr/HRBP (d) Fe+Cr/HRBP

All the applied coatings were first examined visually using an optical microscope. For the initial assessment of paint uniformity, a portable digital microscope equipped with an LED light source and 1600X magnification from CoolingTech was utilized. The thickness of the coatings was measured using an LS220 coating thickness gauge manufactured by Shenzhen Linshang Technology, China. This device offers precise thickness measurements on both ferrous and non-ferrous substrates. Multiple readings were taken for each substrate, and the average value was calculated to determine the coating thickness. Additionally, the coatings were analyzed with a scanning electron microscope (Inspect S50 SEM from FEI, Netherlands), allowing detailed observation of the coating's microstructure and the integration of particles within the composite layers. The coated substrates underwent elemental analysis and mapping using electron energy-dispersive spectroscopy (EDS). This analysis was performed with the XFlash-6l10 detector from Bruker, integrated with the scanning electron microscope. This detector offers excellent resolution ranging from 36 to 122 eV and supports a high pulse load capacity. It enables the detection of low elemental concentrations with a relative precision of 2–5% across a fairly large area. To evaluate and compare the coatings' solar-to-thermal conversion performance, UV-Vis spectroscopy was employed using UV-3600i Plus spectrometer from Shimadzu. The comparison of UV-Vis spectra provides important insights into how the coating components influence their effectiveness as selective coatings and identifies the wavelengths at which incident radiation is absorbed. By analyzing multiple spectra, the extent of radiation absorption at specific wavelengths can be further examined in relation to changes in coating composition (spectral absorbance). The solar-to-thermal conversion of the as-prepared coatings was verified by exposing the substrates to radiation and measuring their temperature with time. Each substrate was placed inside a solar collector as shown in figure 2. The solar collector was made of thermally insulating material. The incident radiation passed through the transparent glass window to the substrate. A thermocouple probe attached to a GM1312 digital thermometer from Benetech from Shenzhen Jumaoyuan Science And Technology Co. Ltd. / China was used to measure the substrate temperature. Temperature measurement was performed every 60 seconds starting from the substrate exposure to radiation until a constant temperature was reached. Two sources of radiation were used in the present work, solar radiation and an artificial source of radiation from a tungsten hot-filament bulb. In the case of an artificial source of radiation, the source-to-collector distance was adjusted such that the total incident irradiance was comparable to that of the solar radiation.

The total reflection of the incoming radiation was determined using a custom-built setup resembling a pyrheliometer, as depicted in Figure 3. This arrangement enabled the measurement of the total reflected radiation relative to the incident radiation, while excluding any diffuse reflection. An SM206-SOLAR digital solar-power meter from Hangzhou Yucheng Industrial Co., Ltd. (China) was employed to record the irradiance levels. During the reflectance measurements, the setup was adjusted so that the incident radiation struck the substrate surface at a 45-degree angle. This positioning ensured that most of the reflected radiation was directed perpendicularly onto the detector of the power meter. The total reflectance values obtained from the substrates can be directly correlated with the UV-Vis spectral data. Understanding the total reflectance is crucial for interpreting the solar-to-thermal conversion performance of the coated substrates.

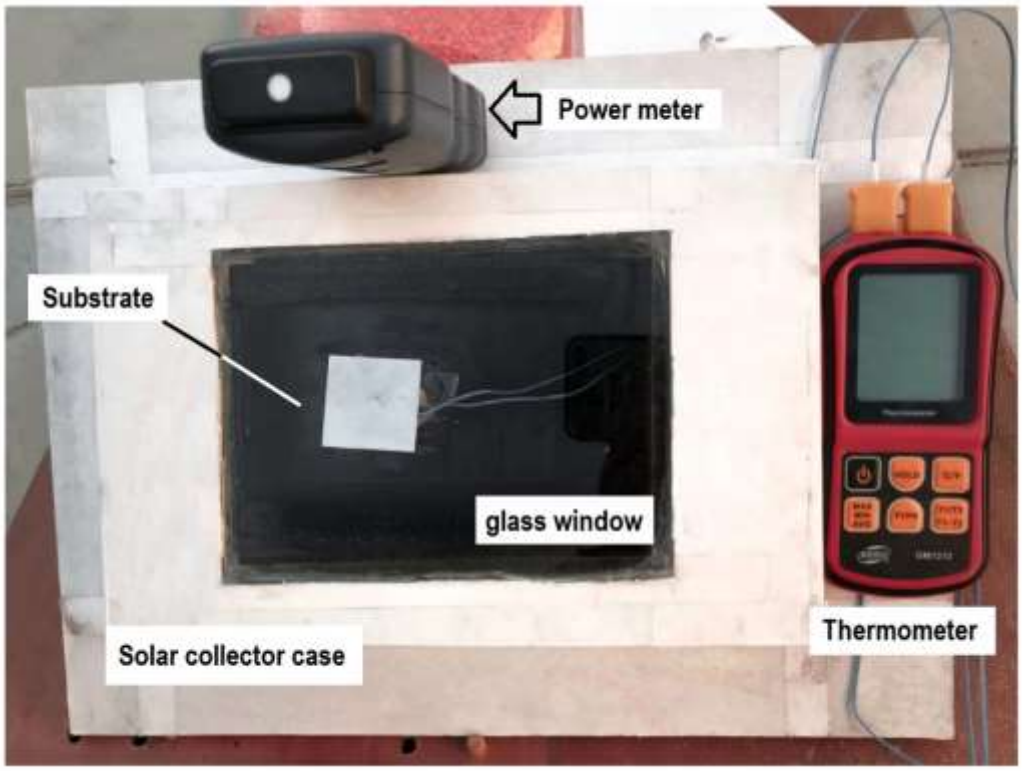

Figure 2: The Solar-Collector setup.

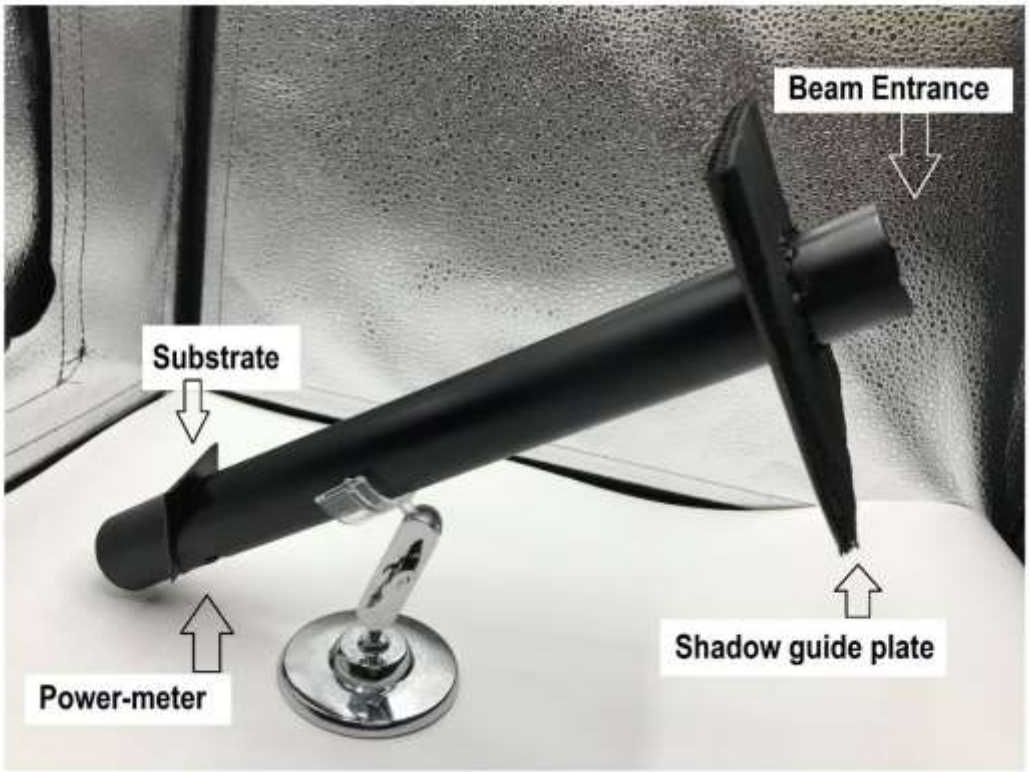

Figure 3: The custom-built of a pyrheliometer-like setup.

3. Results and Discussion

Photographs of the coated aluminum substrates are displayed in Figure 1. These images demonstrate that the coatings were evenly and fully applied to one surface of each substrate. The opposite side remained uncoated and served as a surface for measuring the substrate's temperature. The powders used in the present work, namely, Fe and Cr powders are examined under scanning electron microscope as shown in figure 4. Figure 4 (a), SEM of Fe powder, shows a collection of irregularly shaped, plate-like particles distributed across the field of view. The image was captured at a magnification of 2000X and exhibited with a scale bar of 50 micrometers (μm). The accelerating voltage used was 30 kV, and the working distance was 25.2 mm. The particles appear as angular, flaky, and layered structures, with sizes ranging from a few micrometers up to several tens of micrometers. Many of the particles have sharp edges and a rough surface texture, suggesting a brittle or crystalline nature. The particles are densely packed, with some overlapping and others lying flat or at various angles. This arrangement creates a complex, three-dimensional microstructure. The surfaces of the flakes show fine details, including ridges, steps, and occasional small fragments attached to larger particles. Some particles appear to have undergone fracturing or cleavage, exposing fresh surfaces. This may be attributed to the processing of powder after its synthesis. The high magnification and good contrast highlight the fractured nature of the material, which is typical for the mineral powder. Figure 4 (b), the SEM image of chromium powder, was captured at an accelerating voltage of 30.00 kV and a working distance of 25.1 mm. The Cr powder consists of irregularly shaped particles, with sizes ranging from a few micrometers up to approximately 50 μm. The particles exhibit a generally angular to sub-angular morphology, with some larger, blocky aggregates surrounded by smaller fragments. The surfaces of the particles are notably rough and uneven, displaying a highly textured, almost porous appearance. Many particles have fine, flake-like protrusions or smaller particles loosely attached to their surfaces, which may indicate a degree of agglomeration or secondary particle formation during powder processing. The particles are densely packed and randomly oriented within the field of view, with some overlapping and others lying adjacent. This random arrangement creates a complex, three-dimensional network, typical for metallic powders prepared by mechanical or chemical methods. The presence of smaller particles attached to larger ones suggests some degree of agglomeration, which is common in fine metallic powders and can affect flowability and packing density. The irregular shapes, rough surfaces, and wide size distribution are characteristic of powders produced by mechanical milling or atomization processes rather than by chemical reduction or electrolytic methods, which often yield more uniform particles. The high surface area and roughness of the Cr powder particles can enhance their reactivity, which is beneficial for applications such as powder metallurgy, thermal spraying, or as precursors in composite materials. However, agglomeration may impact the uniformity of compaction and sintering in metallurgical processes. These features are typical for mechanically processed metallic powders and suggest suitability for applications requiring high surface area and reactivity, though care should be taken regarding powder handling and compaction.

The EDS spectrum of the Fe powder (figure 5) shows several peaks corresponding to different elements present in the sample. The main element identified is iron with prominent peaks at approximately 6.4 keV (Kα) and 7.1 keV (Kβ), indicating that it is the dominant element in the sample as expected for Fe powder. Cobalt was observed with noticeable peaks at around 0.8 keV (Lα) and 6.9 keV (Kα). This suggests that cobalt is a secondary component or a contaminant. It is well-known as fact that cobalt usually present as minor element in Fe-dominating powders. This is because cobalt is intentionally added in small amount to improve specific properties of the powder such as magnetic performance and corrosion resistance. These two elements are compatible with each other as they form solid solution over wide range of composition. Low concentration of cobalt improves certain properties without altering the iron matrix significantly [19]. Platinum (Pt) showed peaks at approximately 2.05 keV (Mα), 9.4 keV (Lα), and lower energies, likely originating from the Pt coating commonly used to make non-conductive samples suitable for SEM/EDS analysis. Carbon showed a small peak at around 0.27 keV, which may be due to contamination. Aluminum showed a small peak at around 1.5 keV, from the substrate. The Fe powder is primarily composed of iron, with minor cobalt content. The spectrum suggests high purity iron powder with minor cobalt and negligible contamination from other elements.

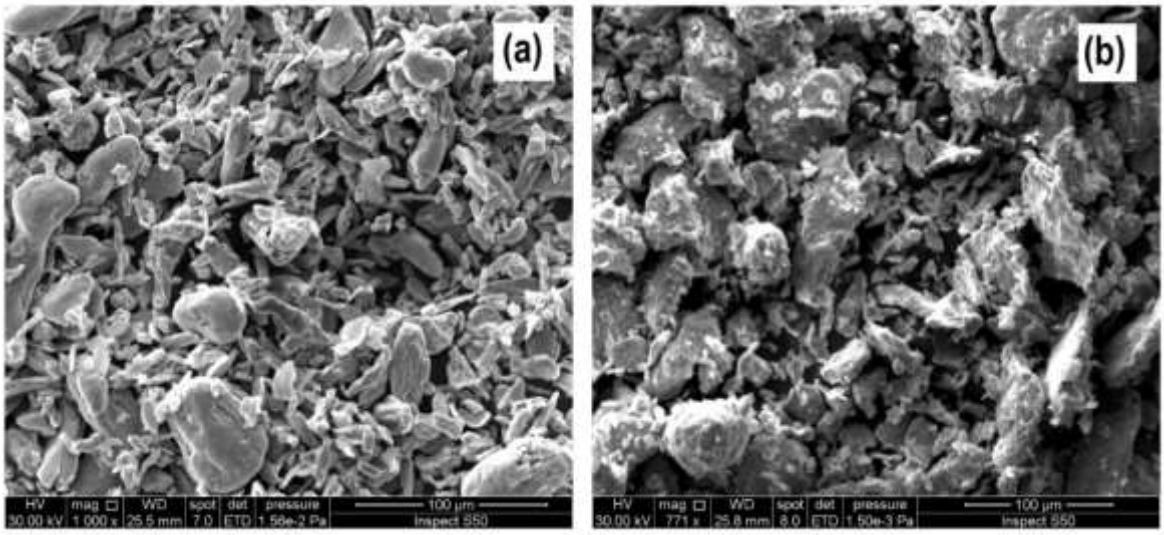

Figure 4: The SEM images of (a) Fe powder (b) Cr powder.

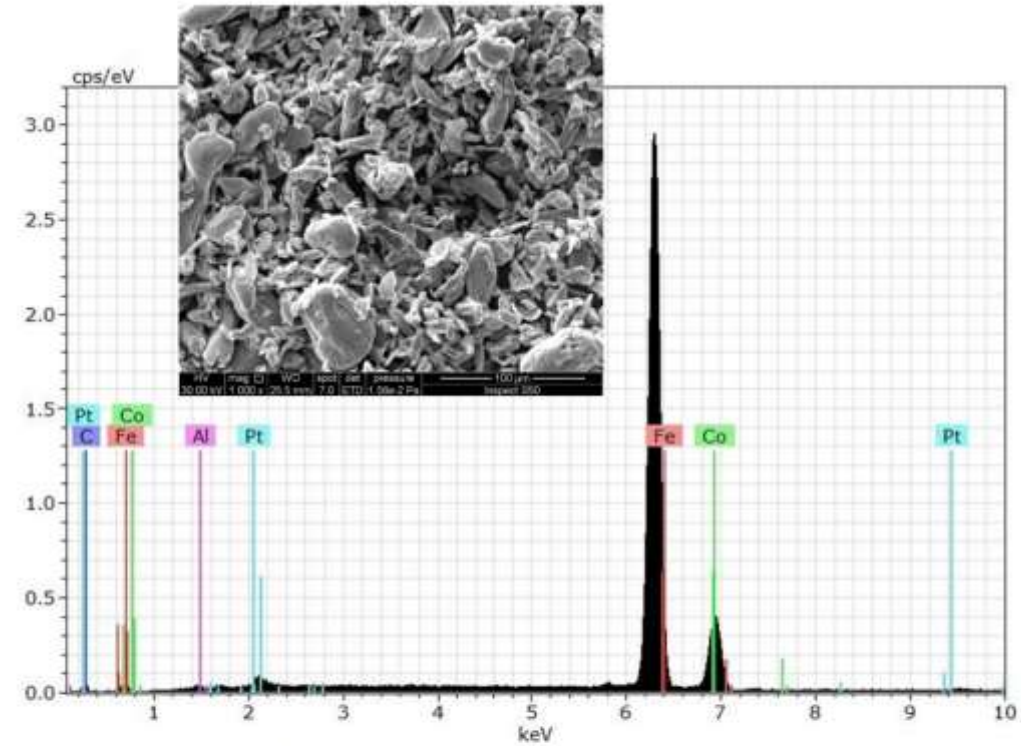

Fe Powder

El	AN	Series	unn. C [wt.%]	norm. C [wt.%]	Atom. C [at.%]	Error (1 Sigma) [wt.%]
Fe	26	K-series	30.59	61.15	42.99	0.81
Co	27	K-series	11.85	23.69	15.78	0.34
C	6	K-series	6.07	12.13	39.66	1.44
Pt	78	L-series	1.14	2.28	0.46	0.08
Al	13	K-series	0.38	0.76	1.10	0.06
		Total:	50.03	100.00	100.00	

Figure 5: The EDS spectrum of the Fe powder.

The EDS spectrum of Cr powder is shown in figure 6. High intensity peaks were observed near 5.41 keV which is characteristic of the chromium element. Another peak near 5.9 keV was identified and attributed to presence of manganese as second element. The presence on Mn as minor element in Cr-dominating powder is due to their mineral association and chemical behavior during processing. Chromium is known to reflect a geochemical affinity that dominates the mineral structure. Chemical processing during powder production may result into Mn being a minor phase or impurity [20].

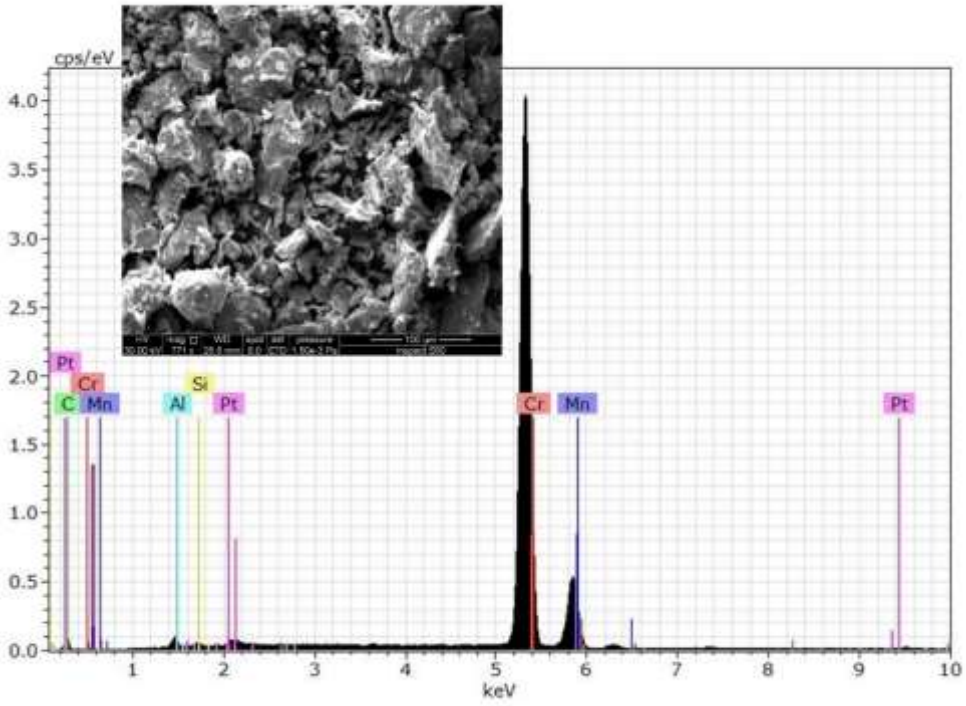

Cr Powder

El	AN	Series	unn. C [wt.%]	norm. C [wt.%]	Atom. C [at.%]	Error (1 Sigma) [wt.%]
Cr	24	K-series	29.66	67.60	42.48	0.81
C	6	K-series	7.63	17.39	47.30	1.58
Mn	25	K-series	4.09	9.32	5.55	0.14
Al	13	K-series	1.31	2.99	3.62	0.11
Pt	78	L-series	0.92	2.10	0.35	0.07
Si	14	K-series	0.26	0.60	0.70	0.05
		Total:	43.87	100.00	100.00	

Figure 6: The EDS spectrum of the Cr powder

Figure 7 shows the uncoated and as-coated substrates observed under scanning electron microscope. An initial examination of the uncoated substrate (figure 7 (a)) reveals unidirectional grooves caused by the brush cleaning process. After applying the primary coating (HRP), these grooves become less noticeable as they are filled in with the coating material (Figure 7 (b)). These grooves lead to enhanced adhesion of coating with the aluminium substrate thus durability of coating. Figure 7 (c and d) show the coated substrates where Fe and Cr powders added on the top of the primary paint layer respectively. As compared with the substrate coated with the primary paint (i.e. Figure 7 (b)), the addition of the Fe and Cr particles led to rougher and more heterogeneous surfaces (figure 7(e)). The particles are dispersed constantly across the surface. The particles vary in size and shape, with some appearing as flakes or clusters, and are clearly distinguishable from the smoother underlying paint. The surface area and roughness are significantly increased due to the presence of these particles. These surface

features can affect the optical, electrical, and mechanical properties of the coating, such as reflectivity and adhesion characteristics. The photo-thermal conversion characteristics are also likely to change due to modification of surface features. This will be investigated in the subsequent measurements.

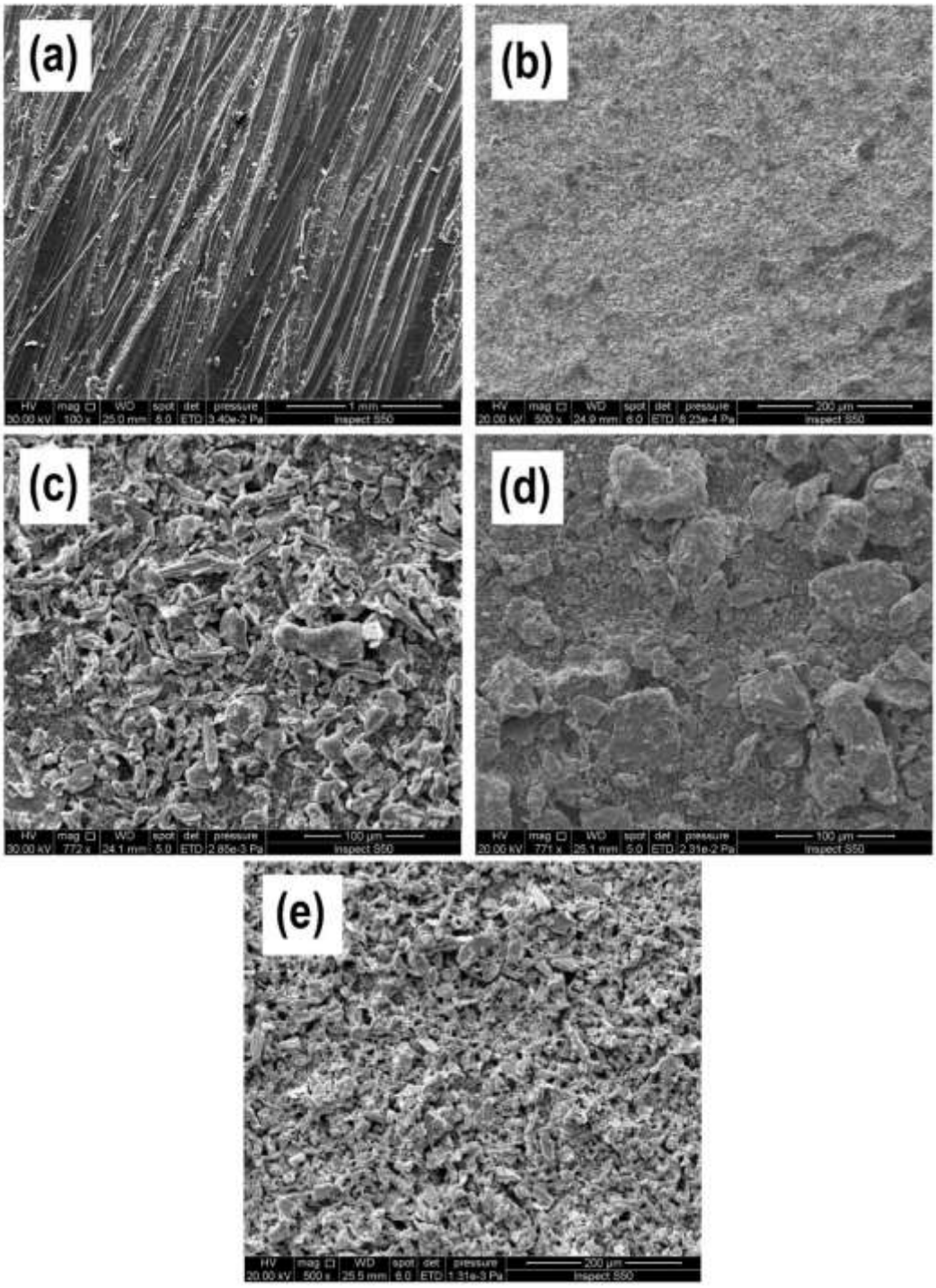

Figure 7: SEM images of the substrates (a) Uncoated Al substrate, and as coated with (b) HRBP (c) Fe/HRBP (d) Cr/HRBP (e) Fe+Cr/ HRBP

Considering the resemblance in coatings preparation and imaging conditions, the Fe-containing coating tends to produce higher-contrast images than the Cr-containing coating. This might be attributed to the fact that Backscattered electrons are more strongly emitted from elements with higher atomic numbers (i.e. iron), producing brighter areas in SEM images [21]. Additionally, Fe powders often exhibit more pronounced surface oxidation or corrosion products, which can further enhance contrast due to compositional and topographical differences. Figure 7 (e), where Fe and Cr powders are added together on top of the paint, shows common features to those observed in figure 7 (c and d) with a moderate contrast. The complexity of the surface morphology affects its photo-thermal conversion efficiency by influencing light absorption, scattering and heat generation on the material's surface. Light trapping increases with corrugations and micro- to nano-scale roughness via multiple internal reflection of incident light. Complex features lead to larger surface areas. In addition, such morphologies can influence thermal conductivity and heat dissipation, affecting the overall photo-thermal performance [22]. Table 2 presents the results of elemental analysis of the coated substrates as determined by energy-dispersive X-ray spectroscopy. It is evident that more elements are detected in the heat-resistant black paint (HRBP) than in the Fe+Cr/HRBP sample. This can be attributed to the fact that, during EDS analysis in SEM mode, the effective sampling depth is typically between 0.5 and 3 µm. Given that the total coating thickness ranges from 20 to 35 µm, EDS primarily analyzes the uppermost layers [23]. As a result, the addition of Fe and Cr powders on top of the HRBP limits the detection of elements from the underlying paint, leading to a reduced number of detected elements in the Fe+Cr/HRBP sample (see Table 1). While the Fe/HRBP sample shows insignificant presence of chromium the Cr/HRBP shows presence of iron. This might be attributed to a combination of multiple factors. The detection limit and sensitivity depends on the atomic number of the element and the detection time. In addition cross-contamination or diffusion effects may play a role in this detection. Some intermixing or diffusion of Fe and Cr between layers during coating or heat treatment could lead to the presence of iron in the Cr/HRBP sample, explaining the detection of Fe where Cr was added [24]. The Fe+Cr/HRBP sample exhibits weight percentages of iron and chromium that are consistent with the proportions used in our coating preparation. The presence of silicon and magnesium is attributed to magnesium silicate in the black paint, while the detected carbon originates from the acetone and propane components of the paint (see table 1).

Table 2: Normalized weight percentage of elements detected in coatings by EDS

Element	Atomic No.	Coating			
		HRBP	Fe/HRBP	Cr/HRBP	Fe+Cr/HRBP
		Normalized Wt.%	Normalized Wt.%	Normalized Wt.%	Normalized Wt.%
Cr	24	4.64	-	46.28	50.889
Fe	26	5.00	65.34	10.59	42.587
Si	14	72.12	16.40	18.14	6.522
Mg	12	9.96	6.66	5.91	-
Se	34	8.27	-	-	-
C	6	-	-	19.07	-
Co	27	-	22.16	-	-
Total		100%	100%	100%	100%

The photo-thermal conversion performance of the prepared coatings was measured under the exposure to solar radiation. Results are presented in figure 8. The solar irradiance during the measurements was 1160±25 W/m^2. The substrate temperature exhibited a notable increase over the duration of exposure. Initially, the temperature increased sharply from ambient temperature due to the efficient conversion of radiation into thermal energy combined with minimal energy loss from the substrate surface. However, after approximately ten minutes, the rate of temperature increase began to diminish, causing the temperature curve to gradually level off. Ultimately, after 25 minutes of continuous exposure, the substrate temperature reached a steady maximum, indicating that the rate of heat gained from the radiation had balanced the rate of thermal energy losses. Figure 5 illustrates that the substrate

coated with Fe/HRBP reached a higher temperature of 364.75 K. In contrast, the coating containing chromium demonstrated slightly lower photo-thermal conversion performance, which may be due to the intrinsic spectral absorption properties of chromium particles compared to those of iron particles. Previous studies have shown that Fe particles exhibit higher absorption characteristics to solar radiation [22]. The coating composed of both iron and chromium powders exhibits slightly lower photothermal conversion compared to the coating containing only iron powder. This difference is attributed to the lower conversion efficiency of chromium relative to iron. The elemental ratios obtained from the EDS measurements (table 1) are consistent with these findings. Table 3 presents the absorptance values for the four coatings studied, as determined from total reflection measurements conducted with the Pyrheliometer-like setup. The Fe/HRBP shows highest absorptance relative to the other coatings. These values agree with the photo-thermal conversion measurements and will be addressed in the subsequent discussion.

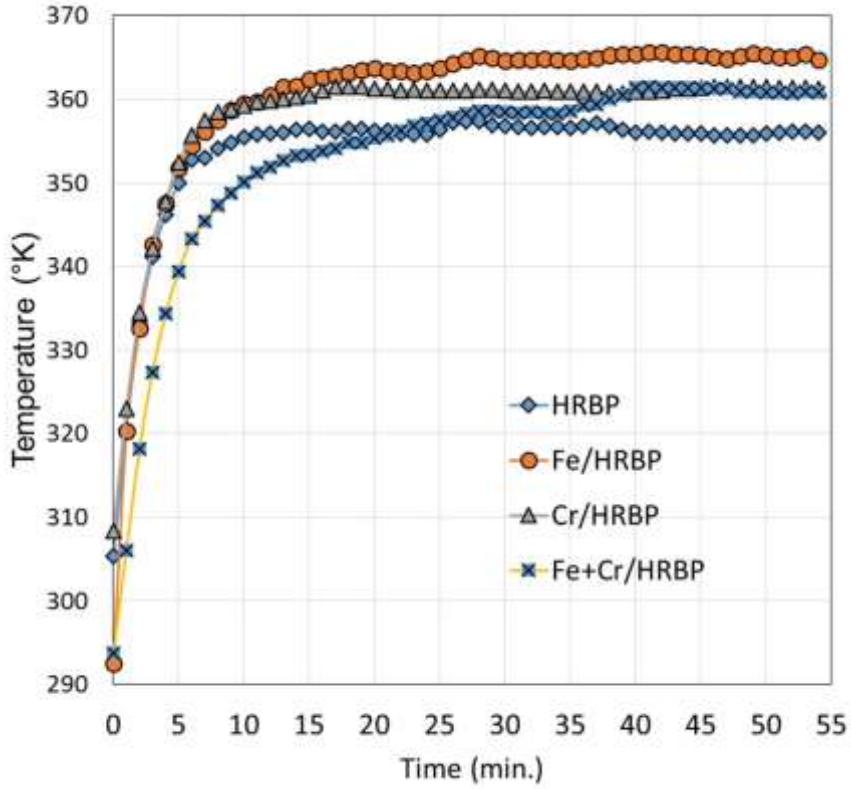

Figure 8: The photo-thermal conversion performance of the coatings under solar irradiation.

Table 3: Absorptance of coatings as determined from the total reflection measurements.

Coating	Total Solar Irradiance W/m²	Beam Irradiance W/m²	Reflected power W/m²	Absorptance (%)
HRBP	933.8	747.3	33.3	95.54
Fe/HRBP			28.1	96.23
Cr/HRBP			29.1	96.10
Fe+Cr/HRBP			32.1	95.70

To better understand the photo-thermal conversion of the coatings, their spectral absorptance was measured using UV-visible absorption spectroscopy. Figure 9 presents a comparison of the spectral absorptance of the coatings over the wavelength range of 200 to 1000 nm of the incident radiation. All coatings show a pronounced peak in absorptance between approximately 500 nm and 800 nm, with the

maximum around 650 nm. The Fe/HRBP coating (orange) exhibits the highest absorptance, followed by HRBP (blue), Cr/HRBP (green), and Fe+Cr/HRBP (light blue). This suggests that adding Fe increases the reflectance of the HRBP coating. The Cr/HRBP has a lower peak reflectance than Fe/HRBP but higher than the Fe+Cr/HRBP, indicating moderate reflectance enhancement by Cr. As the Fe+Cr/HRBP exhibits the lowest absorptance at the main peak, suggesting a synergistic effect when both Fe and Cr are present, leading to optimized absorption. In the UV region (200–400 nm), all coatings have very low absorptance, indicating weak absorption in this range. Nevertheless, absorption of the incident radiation rises sharply in the visible region with clear dependence on the coating composition. The peaks observed in the UV-Vis spectra of figure 9 suggest that absorption of incident radiation involves electronic transitions that are characteristic of the materials involved (i.e. the transition metals of iron and chromium). Absorption bands are known to arise from the d-d transitions, where an electron in the lower-energy d orbital is excited to a higher-energy d orbital within the same metal ion. These transitions are typically spin- and Laporte-forbidden, so they are weaker but still contribute to the visible absorptance and color of metal-containing coatings (responsible of the black appearance of the coating). These peaks may also be attributed to metal-to-ligand charge transfer. This involves electron transfer between metal ions and surrounding matrix materials. Such transitions tend to be strong and often contribute to broad absorption bands [25-27]. No prominent peaks were observed in the UV region (200 – 400 nm). This may indicate weak contribution of π – π* transitions that occur in conjugated double bonds [28].

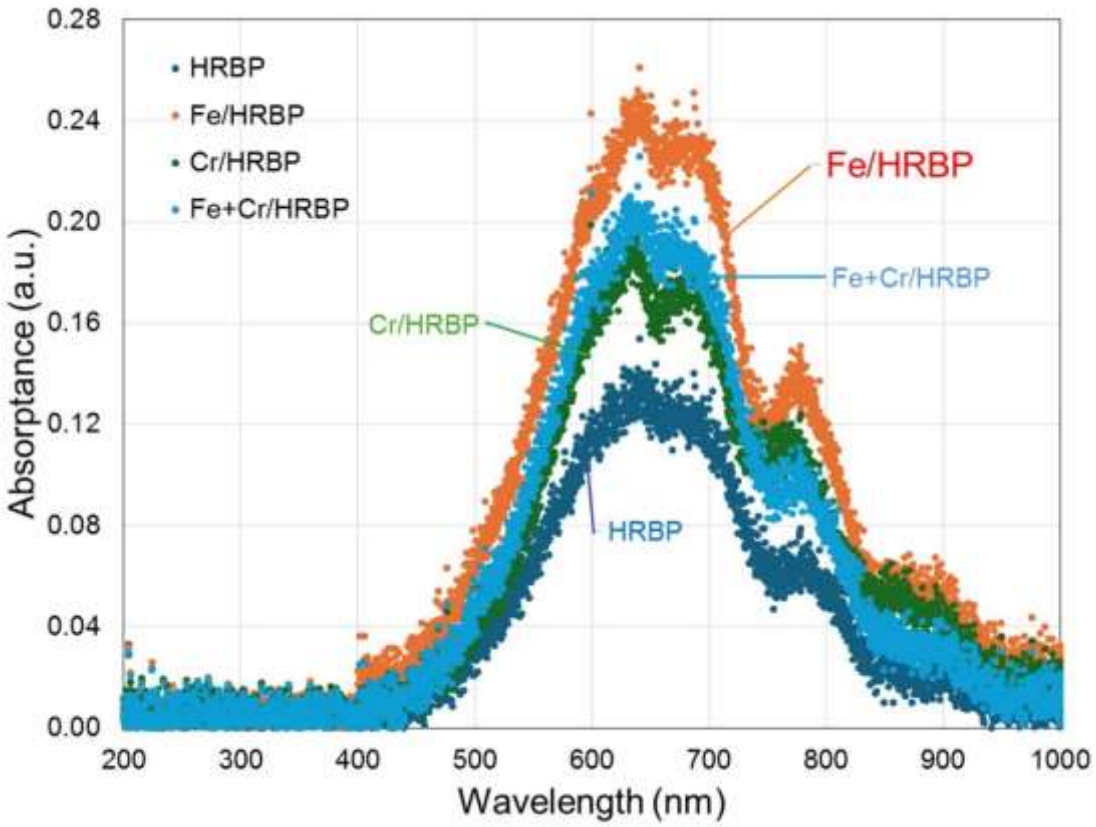

Figure 9: Comparison of the spectral absorptance of the coatings.

The four spectra presented in Figure 9 exhibit similar absorption peak positions, indicating that the same absorbing species and functional groups are involved in the photo-thermal conversion of the coatings. However, the intensity of these peaks differs depending on the coating composition. This variation in peak intensity directly reflects the differing concentrations of these species and functional groups

within each coating. Compared to the HRBP, incorporating iron and chromium into the coating was found to improve its photo-thermal conversion efficiency. This clarifies why there is a higher rate of solar radiation being converted into heat in the Fe/HRBP coating. The area under the curve of a UV-Vis spectrum represents the integrated absorbance over the specified wavelengths [29-31]. This quantifies the total light absorption allowing for optimization of the constituents concentrations within the coating. Table 4 presents the integrated absorbance values over designated wavelength ranges for the four coatings studied. The first three columns correspond to the areas under the curve for the first, second, and third absorption peaks, respectively. The final column shows the total integrated area under the entire spectrum, representing the overall absorbance. The results indicate that the Fe/HRBP coating exhibits the largest integrated absorbance areas, while the HRBP coating shows the smallest. This suggests that incorporating iron particles into the primary coating improves its absorption properties, resulting in the most efficient conversion of solar energy into heat. These findings align with the photo-thermal conversion data obtained from the solar collector system. The highest temperature recorded for the Fe/HRBP coating can be correlated with the integrated absorbance values derived from the area under the curve, as discussed earlier.

Table 4: Integrated absorbance over specified wavelength of the incident radiation.

	Area under the curve (a.u.) over specified wavelength			
Coating	600 – 650 nm	650 – 710 nm	750 – 800 nm	200 – 1000 nm
HRBP	6.38	7.40	3.09	31.08
Fe/HRBP	11.62	13.7	6.48	60.10
Cr/HRBP	8.97	10.16	5.29	45.29
Fe+Cr/HRBP	9.75	11.21	4.72	46.84

State-of-the-art spectrally selective coatings are engineered to achieve high absorptance in the visible and near-infrared wavelengths for efficient solar energy absorption, while minimizing absorptance at longer wavelengths to reduce thermal emission losses. Multilayer coatings accomplish this by stacking alternating layers with different refractive indices, producing sharp or broad absorption bands optimized for high solar absorptance (often exceeding 0.90) and low thermal emittance [32]. These coatings typically exhibit smooth, reproducible spectral features due to their precise fabrication methods. While multilayers provide superior spectral selectivity and solar thermal performance, HRBP-based coatings with Fe and Cr additives offer a simpler and more cost-effective alternative for applications where extreme performance is not critical. The absorptance spectra shown in Figure 9 can also be related to the morphological characteristics of the coating surfaces depicted in Figure 4. It appears that the surface complexity has a direct impact on the photo-thermal conversion performance of the coatings. Specifically, the Fe/HRBP coating exhibits more intricate morphological features compared to the Cr/HRBP, which corresponds to its superior photo-thermal conversion efficiency. As previously noted, these characteristics suggest that the enhancement of the coating's functional performance is primarily due to the trapping of incident radiation and multiple internal reflections. It is important to highlight that the coatings examined were tested multiple times over a period exceeding eight months. Throughout this duration, no significant changes in appearance, degradation, or functional performance were observed. In practical applications, these coatings are not intended to endure aggressive environmental corrosion or mechanical wear. The primary factors affecting them are exposure to UV radiation and adhesion challenges arising from substrate temperature fluctuations. Our observations revealed no notable degradation linked to these influences. The long-term stability of the present coatings is closely linked to the durability of the heat-resistant paint used. For spectrally selective coatings, maintaining optical and structural integrity under prolonged exposure to high temperatures, thermal cycling, and environmental conditions is critical.

4. Conclusions

In conclusion, this study demonstrates that incorporating iron (Fe) powder into heat-resistant black paint coatings on aluminum substrates significantly enhances solar-to-thermal conversion. The addition of Fe and chromium (Cr) powders alters the surface morphology by increasing roughness and complexity, thereby improving light trapping and absorption. Among the tested coatings, the Fe-

modified paint exhibited the highest solar absorptance (96.23%) and achieved the greatest temperature rise under solar irradiation, outperforming both Cr-modified and combined Fe+Cr coatings. Spectral analysis confirmed that Fe-containing coatings possess superior integrated absorbance in the visible range, directly correlating with their enhanced photo-thermal performance. These findings establish that Fe-enhanced coatings provide a practical and effective strategy for maximizing solar energy conversion on aluminum substrates, with significant potential for advancing the efficiency of solar thermal collector technologies.

Conflict of Interest: The authors declare no conflict of interest pertaining this research.

Funding: No funding was received for this work.

References

[1] Kalogirou, S.; "Solar thermal collectors and applications". Prog. Energy Combust. Sci. 30: 231-295, 2004.

[2] Muhammad Zain, Muhammad Amjad, Muhammad Farooq, Zahid Anwar, Rabia Shoukat, Enio P. Bandarra Filho, Xiaoze Du; "Performance Investigation of a Solar Thermal Collector Based on Nanostructured Energy Materials". Front. Mater. 7: 617199, 2021.

[3] Carrión-Chamba, W.; Murillo-Torres, W.; Montero-Izquierdo, A.; "A review of the state-of-the-art of solar thermal collectors applied in the industry". Ingenius, Rev. Cienc. Tecnol. N.◦ 27, pp. 59-73, 2022.

[4] Opoku, K. N.; Wei, Y.; Dankwa, C. A. A.; Ni, R.; Wang, Z.; Zhai, L.; Zhang, J.; Ang, E. H.; Yang, F.; "Advances in photothermal water evaporation: synthesis, mechanisms, and coupled techniques". Energy Mater. 5: 500020, 2025.

[5] Aquilanti, A.; Peralta, I.; Koenders, E. A. B.; Di Nicola, G.; "A Brief Review of the Latest Advancements of Massive Solar Thermal Collectors". Energies 16: 5953, 2023.

[6] Xiao, X.; Wei, X.; Wei, J.; Wang, J.; "Multifunctional Fe3O4-based photothermal superhydrophobic composite coating for efficient anti-icing/deicing". Sol. Energy Mater. Sol. Cells 256: 112313, 2023.

[7] Li, C.; Goswami, Y.; Stefanakos, E.; "Solar assisted sea water desalination: A review". Renew. Sustain. Energy Rev. 19: 136-163, 2013.

[8] Ding, Z.; Qi, C.; Wang, Y.; Tu, J.; Wang, C.; Du, X.; "Spectrally selective absorption coatings and their applications: A review". Sustain. Energy Technol. Assess. 52(A): 102031, 2022.

[9] Kumar, K. R.; Krishna Chaitanya, N. V. V.; Sendhil Kumar, N.; "Solar thermal energy technologies and its applications for process heating and power generation – A review". J. Clean. Prod. 282: 125296, 2021.

[10] Olabi, A. G.; Shehata, N.; Maghrabie, H. M.; Heikal, L. A.; Abdelkareem, M. A.; Atiqure Rahman, S. M.; Shah, S. K.; Sayed, E. T.; "Progress in Solar Thermal Systems and Their Role in Achieving the Sustainable Development Goals". Energies 15(24): 9501, 2022.

[11] Zayed, M. E.; "Recent Advances in Solar Thermal Selective Coatings for Solar Power Applications: Technology Categorization, Preparation Methods, and Induced Aging Mechanisms". Appl. Sci. 14: 8438, 2024.

[12] Zeng, X.; Long, Z.; Liu, Z.; Cao, Q.; Cheng, X.; "Preparation and Characterization of Co-CuCoMnOx Solar Selective Absorption Coatings". Coatings 15(547): 2-16, 2025.

[13] Chen, Z.; "Carbon Nanotube Spectrally Selective Solar Thermal Absorbers". Ph.D. Dissertation, Department of Physics and Technology, Faculty of Science and Technology, The Arctic University of Norway, 2016.

[14] Chen, Z.; Nguyen, Q. H.; Boström, T.; "Carbon Nanotube Spectrally Selective Solar Absorbers". Proceedings of the ISES EuroSun 2014 Conference, France, pp. 806-813, 2015.

[15] Zäll, E.; Segervald, J.; Mahmoodi, H.; Perivoliotis, D.; Edman, L.; Wågberg, T.; "Achieving optically selective coatings of silica fixated carbon nanotubes for solar energy applications". Sol. Energy Mater. Sol. Cells 278: 113202, 2024.

[16] Jasim, R. H.; Al-Tabbakh, A. A.; "Enhancement of the Solar-Thermal Response of Flat-plate Collector Coated with a Heat-resistant Paint". Jordan J. Phys. 15(3): 323-329, 2022.

[17] Jasim, R. H.; Al-Tabbakh, A. A.; Hasan, S. M.; "Improvement of the Solar-Thermal Characteristics of the Flat-Plate Collector Using a Composite Coating". Al-Nahrain J. Sci. 24(1): 14-19, 2021.

[18] Fernández-Afonso, Y.; Asín, L.; Pardo, J.; Fratila, R. M.; Veintemillas, S.; Morales, M.

P.; Gutiérrez, L.; "Magnetic iron oxide nanoparticles for photothermal therapy: physicochemical properties, irradiation power, and particle concentration in vitro". Nanoscale Adv. 7: 336–345, 2025.

[19] Fraser, R. W.; Evans, D. J. I.; "The Properties Of Cobalt-Iron Alloys Prepared By Powder Rolling". Powder Metall. 11(22): 358-378, 1968.

[20] Fleischer, M.; Mandarino, J. A.; "Glossary of Mineral Species 1995 (7th Edition)". The Mineralogical Record, Inc., Tucson, AZ, 280 p., 1995.

[21] Gao, Y.; Liu, R.; "Removal of Cr(VI) from groundwater by Fe(0)". Appl. Water Sci. 7: 3625–3631, 2017.

[22] Dutraa, K. H.; Freirea, F. N. A.; Pinhoa, D. C.; Araújoa, F. A. A.; "Characterization of a Selective Surface Based on Chromium, Iron and Aluminum Oxides for Application in Solar-Thermal Collectors". Mater. Res. 25: e20210489, 2022.

[23] Microscopy Australia; "Energy Dispersive Spectroscopy". MyScope Microscopy Training, www.myscope.training.

[24] von Harrach, H. S.; Klenov, D. O.; Freitag, B.; Schlossmacher, P.; Collins, P. C.; Fraser, H. L.; "Comparison of the detection limits of EDS and EELS in S/TEM". Microsc. Microanal. 16 (Suppl 2): 1312-1313, 2010.

[25] Farley, J. W.; Brumley, W. C.; Eastwood, D.; "Electronic Spectroscopy, Environmental Applications". Encycl. Spectrosc. Spectrom. (3rd Ed.): 452-458, 2017.

[26] Miessler, G. L.; Tarr, D. A.; "Inorganic Chemistry", 3rd ed.; Pearson Education Inc: New Jersey, 2004; p. 390.

[27] Sinha, N.; Wenger, O. S.; "Photoactive Metal-to-Ligand Charge Transfer Excited States in 3d6 Complexes with Cr0, MnI, FeII, and CoIII". J. Am. Chem. Soc. 145: 4903−4920, 2023.

[28] LibreTexts; "Chemistry Library". https://chem.libretexts.org.

[29] Gadhave, M. V.; Badhe, N.; Jadhav, S. L.; Gaikwad, D. D.; Dhobale, S. M.; Gaware, R. U.; "Area Under Curve by UV Spectrophotometric Method for Determination of Ascorbic Acid in Bulk". Bull. Environ. Pharmacol. Life Sci. 9(8): 35-39, 2020.

[30] Sarang, W.; Udmale, D.; Patel, S.; Chordiya, B.; "Area Under Curve UV Spectrophotometric Method for Determination of Valsartan in Bulk". Int. Res. J. Eng. Technol. 6(5): 1044–1048, 2019.

[31] Dhumane, S. A.; Patel, S. G.; Kedar, V. D.; "Area Under Curve by UV Spectrophotometric Method for Determination Aloe Vera Gel Powder in Bulk". Int. J. Res. Anal. Rev. 7(1): 903-909, 2020.

[32] Zhou, Z. H.; He, C. Y.; Ga, X. H.; "Recent advances of spectrally selective absorbers: Materials, nanostructures, and photothermal power generation". APL Energy 2: 011503, 2024.